

## THE STRATEGY FOR MULTI-VIEW DENSE IMAGE MATCHING AND POINT CLOUD REFINEMENT

Hsuan-Hsuan Liu (1), Jen-Jer Jaw (2)

<sup>1,2</sup> Department of Civil Engineering, National Taiwan University,  
No. 1, Sec. 4, Roosevelt Rd., Taipei 10617, Taiwan.  
Email: [r07521808@ntu.edu.tw](mailto:r07521808@ntu.edu.tw); [jejaw@ntu.edu.tw](mailto:jejaw@ntu.edu.tw)

**KEY WORDS:** Dense image matching, Multi-view, Point cloud, Refinement

**ABSTRACT:** Point clouds are increasingly employed as a prime data source for 3-D geo-information related applications. Point cloud generated through dense image matching has recently gained its popularity in depicting 3-D scene through estimating disparity, depth information, of a stereo pair on pixel-wise basis. Considering the geometry and complexity of the scene, it is necessary to configure image acquisition in way of multiple views with highly overlapping requirement in favor of stereo image matching. Yet, an efficient as well as effective way of conducting dense image matching through multiple views and refining the point cloud to well depict the scene still awaits implemented. This study presents a strategy for improving calculation efficiency and reconstruction quality, focusing on delivering reliable disparity values between different pairs and attributing the point cloud. By fixing the chosen reference image, the stereo pairs are sequentially formed with increasing baseline, thus providing the better intersection geometry. And the initial disparity propagated from the first pair for the second pair afterwards gains good prediction with narrower searching area to not only reduce the computational load but also higher the disparity reliability. The combined effect by the proposed approach brings smoothing effect in disparity continuous areas and sharpens the geometric features. Moreover, not only the 3-D coordinates and the precisions of the point clouds have been calculated through intersection of the conjugate points, but also the feature attribute for each point has been assigned based on the geometric information analyzed when executing dense image matching and point clouds. With all of these, mistaken points in point clouds can be removed or weakened for their follow-up applications, and the refinement of point cloud can be realized by using less points to well preserve scene geometry on specific demand.

### 1. INTRODUCTION

The 3-D scene or object reconstruction through dense point clouds has been seen in various fields, for example, land survey, urban planning, landscape analysis, and even culture heritage survey and preservation (Dall'Asta & Roncella, 2014). Over the past years, LiDAR system has played the major role in providing dense point clouds. With recent advances in computer vision, stereo image matching automatically calculates the disparities of conjugate points on a pixel-wise basis and offers an efficient way of reconstructing the scene. Highly overlapping images are required in favor of stereo matching with scenes delicately described in demand, therefore, image acquisition configured in multiple views becomes a necessity when carrying out 3-D scene/object reconstructions (Haala, 2011; Yan *et al.*, 2016).

Methods of automatic stereo pairs matching can be classified into three categories, local matching, global matching and semi-global matching (Hirschmüller, 2005 and 2008). Currently, semi-global matching (SGM) has been tremendously utilized in 3-D reconstruction tasks as it possesses the advantages of both operational efficiency and sufficient matching accuracy. Many easily accessible software applies dense matching algorithms to produce 3-D geo-information, including SURE, Agisoft PhotoScan, Pix4D, and MicMac, just to name a few. When processing multiple-viewed images, redundant point clouds supply a great amount of data enhancing the scene description, yet the reconstructed integrity also suffers from varied levels of positioning errors owing to the different intersection angles of participated image pairs. Figure 1 shows a plane rendered by multi-pair matched point clouds with significant uncertainty. Furthermore, when matching multiple stereo pairs, it would take long to get disparity values if each pair is to be processed independently (Rothermel *et al.*, 2012). It also shows in our previous study (Liu and Jaw, 2019) that matching in short-baseline pair is easier to achieve high successful rate than that in longer-baseline case. However, the latter would provide higher positioning quality than the former. The breakthrough to this dilemma must tackle the two technical issues: (1) how to deliver the reliable disparity effectively between different pairs; and (2) how to refine the number of point clouds taking the quality and quantity indicators into consideration. Many approaches of matching multiple images have been developed. Some methods tend to preselect for each part of the reconstructed scene in a single pair, satisfying the expected accuracy. Other methods focus on the result of disparity and point clouds due to consistency constraints in depth discontinuities, rejecting outliers and noise in matching (Dominik, 2017).

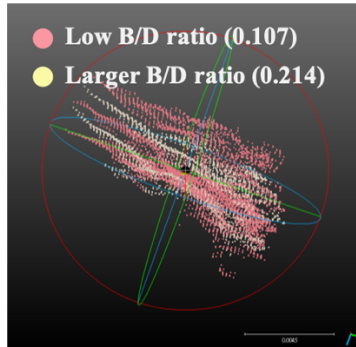


Figure 1. Point clouds of a plane from multi-pair matching (with B the baseline and D the object distance)  
(Modified from (Liu and Jaw, 2019))

To resolve the afore-mentioned two technical issues, an appropriate procedure in optimizing matching algorithms and allowing for fewer point clouds depiction but features preserved has to be proposed. As a result, this study presents a strategy by fixing the chosen reference image, and stereo pairs are sequentially formed with increasing baseline. It follows that the matching from the low base-object distance (B/D) pair would be utilized to predict the corresponding location in longer B/D pair to improve the disparity approximation, making better disparity estimation and more reliable matching result. Besides, both the geometric and radiometric attributes of the points have to be recorded to the subsequent point refinement task. To implement such an idea, an effective estimation and delivery of disparity uncertainty must be arranged and the specific storage of the point cloud has to be designed, which are all to be detailed in the following section.

## 2. METHODOLOGY

The strategy considered for effectively carrying out dense image matching while improving the point cloud quality is proposed to include the several procedures. As it is preferred, the epipolar image pairs are first resampled from the original images. To take a straight forward error propagation treatment, the exterior orientation parameters and errors of the epipolar images are derived based on the transformation from the original to normalized images. The intersections of conjugate points upon stereo matching on a low B/D pair can be directly applied by using epipolar images to obtain the 3-D coordinates of object points and their variance-covariance matrices. With the better information of object points, the corresponding image point locations in the larger B/D pair can be better predicted to narrow down the search extent of disparity, thus making a more efficient and reliable matching realization. The conceptual workflow for the proposed disparity delivery scheme can be seen in Figure 2. The technical implementation is given as follows: Section 2.1 describes epipolar images reconstruction from rotating original images and resampling, and Section 2.2 shows algorithms in matching for obtaining conjugate points. Section 2.3 introduces a mathematical model to provide indicators at point clouds. Section 2.4 presents a strategy to narrow the searching area.

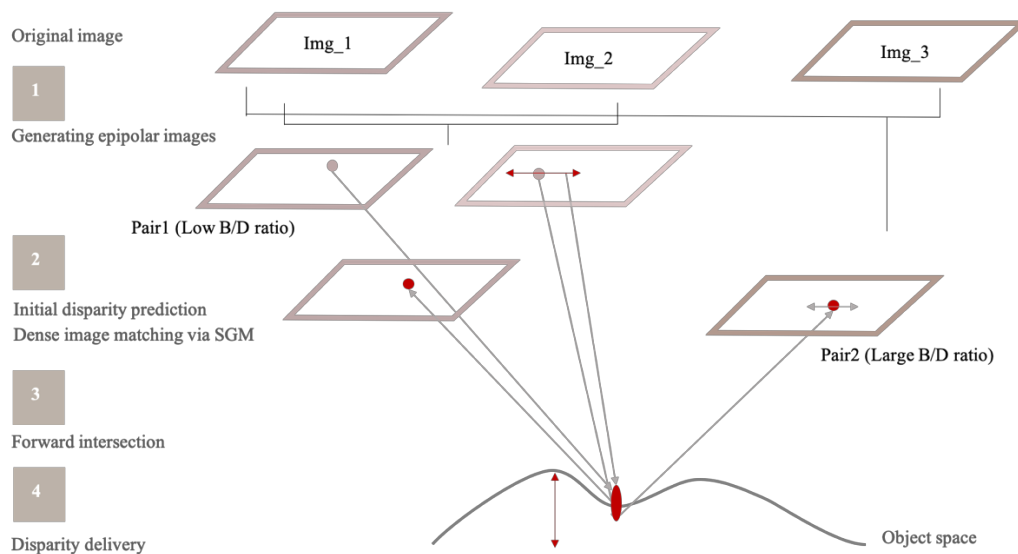


Figure 2. Flow chart of proposed strategy for disparity delivery

## 2.1 Generating Epipolar Images

The construction of epipolar geometry is crucial to enabling the matching along the row direction, deemed as a standard procedure for stereo matching. The transformation introduced in Schenk (1999) from original to epipolar images (or normalized images) is employed. The net effect is to fix the perspective center and rotate the original images to the normalized ones with new but the same angles for the pair. The intensities of the epipolar images are attained by undertaking resampling in the original images. The rotating procedures of making epipolar images and the calculation of corresponding angles are shown in Eqs. (1) to (3):

$$\begin{aligned} M_{Lepipolar} &= M_{baseline} * M_L^T \\ M_{Repipolar} &= M_{baseline} * M_R^T \end{aligned} \quad (1)$$

$$\begin{cases} M_L = M_{L\kappa} * M_{L\varphi} * M_{L\omega} \\ M_R = M_{R\kappa} * M_{R\varphi} * M_{R\omega} \\ M_{baseline} = M_{\theta_X} * M_{\theta_Y} * M_{\theta_Z} \end{cases} \quad (2)$$

where  $(L_\kappa, L_\varphi, L_\omega), (R_\kappa, R_\varphi, R_\omega)$  are the angle sets of left and right original images;  $(\theta_X, \theta_Y, \theta_Z)$  are the angles of epipolar pair and can be computed by Eq. (3).

$$\begin{cases} \theta_X = \omega_{epi} = (L_\omega + R_\omega)/2 \\ \theta_Y = \phi_{epi} = \tan^{-1}(-B_Z / \sqrt{B_X^2 + B_Y^2}) \\ \theta_Z = k_{epi} = \tan^{-1}(B_Y / B_X) \end{cases}, \quad \begin{cases} B_X = X_R - X_L \\ B_Y = Y_R - Y_L \\ B_Z = Z_R - Z_L \end{cases} \quad (3)$$

With  $(X_L, Y_L, Z_L), (X_R, Y_R, Z_R)$  the positions of perspective centers for left and right images, respectively.

Concerning the accuracy and variance-covariance matrix of observations, Eqs. (4) and (5) are employed to perform parameters estimation with  $F$ : functional model;  $l$ : observations, including the perspective centers of and rotation angles with respect to X-axis  $(\omega_L, \omega_R)$ ;  $F_{Jacobi}$ : partial derivative matrix of  $F$  with respect to observations;  $\Sigma_F$ : variance-covariance matrix of observations, the explicit quality estimation of epipolar pair.

$$\begin{aligned} F_{(9*1)} &= [X_L \ Y_L \ Z_L \ X_R \ Y_R \ Z_R \ \theta_x \ \theta_y \ \theta_z]^T \\ l_{(1*8)} &= [X_L \ Y_L \ Z_L \ \omega_L \ X_R \ Y_R \ Z_R \ \omega_R] \end{aligned} \quad (4)$$

$$\Sigma_{F(9*9)} = F_{Jacobi} \Sigma_{l(8*8)} F_{Jacobi}^T = \begin{bmatrix} \sigma_{X_L}^2 & \sigma_{X_L Y_L} & \sigma_{X_L Z_L} & \dots & \dots & \sigma_{X_L \theta_Z} \\ \sigma_{Y_L X_L} & \sigma_{Y_L}^2 & \sigma_{Y_L Z_L} & \dots & \dots & \sigma_{Y_L \theta_Z} \\ \cdot & \cdot & \cdot & \cdot & \cdot & \cdot \\ \cdot & \cdot & \cdot & \cdot & \cdot & \cdot \\ \cdot & \cdot & \cdot & \cdot & \cdot & \cdot \\ \sigma_{\theta_Z X_L} & \sigma_{\theta_Z Y_L} & \sigma_{\theta_Z Z_L} & \dots & \dots & \sigma_{\theta_Z}^2 \end{bmatrix} \quad (5)$$

## 2.2 Dense Image Matching Via SGM

With tremendous progress in photogrammetric and computer vision, the search for conjugate points in a stereo pair is realized by dense image matching algorithms, which divided into four steps: cost computation, cost aggregation, disparity computation and refinement of disparities. This study tackles the sum of absolute difference (SAD) to quantify radiometric quality between images, and smooths disparities through aggregating the neighboring information by semi-global matching. It introduces a modified hierarchical strategy, thus image pyramids, to run efficiently and decrease memory demands (Rothermel *et al.*, 2012). Meanwhile, the quality of disparities is maintained. Then, the Winner Take All (WTA) strategy is applied to choose minimal cost value as its correspondent disparity, and followed by median filter to remove remaining irregularities.

SAD is a function of parametric matching cost in local methods, which assumes brightness constancy for corresponding pixels. The SAD is commonly used with high computation efficiency, especially for the repeated texture images. On the other hand, the weakened object boundaries bringing about unclear depth estimations and readily affected by the slight radiometric differences are the negative side of SAD (Hirschmüller & Scharstein, 2009). Yet, integrating SAD into SGM and going through cost aggregation (Figure 3 (b)) would perform robustly against

outlier that occur in window-based methods. This study executes SGM in eight direction constraints and adds penalty parameters  $P_1, P_2$  for disparity changes, with  $2P_2 = P_1$ .

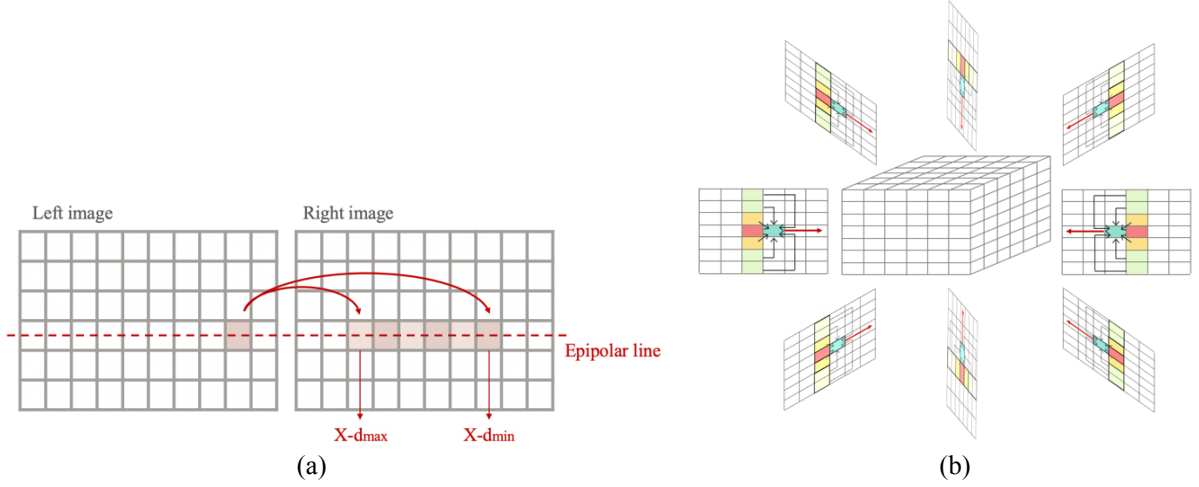


Figure 3. (a) Cost computation, (b) Aggregation in 8 paths

### 2.3 Forward Intersection

After obtaining the depth map from SGM, conjugate points in image pair are found and forward intersection by minimizing observations errors using generalized least-squares adjustment method is implemented to get 3-D coordinates of object points and their variance-covariance matrices. To simplify the expression, let  $G$  represent the collinearity equation of epipolar imagery. The convergent least-squares solutions are determined by Eqs. (6) and (7), with  $B$ : partial derivative matrix of  $G$  with respect to observations;  $A$ : partial derivative matrix of  $G$  with respect the unknowns;  $e$ : vector of error;  $\xi$ : vector of unknowns;  $w$ : vector of discrepancy;  $\Sigma$ : variance-covariance matrix of observations;  $\sigma_0$ : a priori standard deviation of unit weight;  $P$ : weight matrix;  $\hat{\xi}$ : estimation of unknowns;  $\tilde{e}$ : vector of residuals;  $\hat{\sigma}_0$ : a posteriori standard deviation of unit weight;  $r$ : redundancy;  $\hat{\Sigma}_{\xi}$ : a posteriori variance-covariance matrix of estimated unknowns.

$$Be + A\xi = w, e \sim (0, \Sigma = \sigma_0^2 P^{-1}) \quad (6)$$

$$\begin{cases} \hat{\xi} = (A^T (BP^{-1}B^T)^{-1}A)^{-1}A^T (BP^{-1}B^T)^{-1}w \\ \tilde{e} = P^{-1}B^T (BP^{-1}B^T)^{-1}(w - A\hat{\xi}) \\ \hat{\sigma}_0 = \sqrt{\frac{\tilde{e}^T P \tilde{e}}{r}}, \hat{\Sigma}_{\xi(3 \times 3)} = \hat{\sigma}_0^2 (A^T (BP^{-1}B^T)^{-1}A)^{-1} \end{cases} \quad (7)$$

To supply sufficient information for refining point clouds, this study also proposes storing several parameters and indicators to value both the quantity and quality of point clouds. At the current stage,  $\hat{\sigma}_0$ ,  $\hat{\xi}$  and  $\hat{\Sigma}_{\xi}$  are included. Furthermore, Edge Drawing algorithm (Topal & Akinlar, 2012) together with modified SNR indicators (Chiu, 2018) are considered to store the related information of edge features.

### 2.4 Disparity Delivery

According to Eq. (8), where  $f$  is the principal distance of the camera, the disparities of nearest and farthest object distances can be calculated to bound the searching region. Therefore, if the scene knowledge is too rough, the extent of disparity will be too large and easily results in heavy computational load as well as low matching reliability.

$$disparity = f * \frac{B}{D} \quad (8)$$

To cope with the wide search extent of disparity and provide better intersection geometry, the strategy in delivering reliable disparity is fulfilled with propagating the matching result from the low B/D pair to the larger B/D ones. The 3-D coordinates ( $X, Y, Z$ ) of those points intersected from low B/D pair would be projected to the larger B/D pairs to obtain the image locations, specifically for the row ( $x$ ) component, as formulated in Eq. (9). Also the errors of the image locations can be quantified by propagating the associated errors using Eq. (10).

$(X_{epi}, Y_{epi}, Z_{epi}, \omega_{epi}, \phi_{epi}, k_{epi})$ ,  $(x_0, y_0, f)$ , and  $(m_{epi\_11}, m_{epi\_12}, \dots, m_{epi\_33})$  are the exterior orientation parameters, interior orientation parameters, and rotation elements of epipolar image, respectively, while  $H_{Jacobi}$  is the partial derivative matrix of  $H$  with respect to observations. Although each object point has its own uncertainty, thus the disparity error, the estimated disparity extent with the most depth error is adopted and set for the whole target area just for the current implementation to simplify the computation. Nevertheless, the range of disparity uncertainty through the proposed approach would gain effective reduction and benefit the SGM result with more success and higher reliability, as demonstrated in the following experiments.

$$H_{(1*1)} = x_a = x_0 - f \frac{m_{epi\_11}(X - X_{epi}) + m_{epi\_12}(Y - Y_{epi}) + m_{epi\_13}(Z - Z_{epi})}{m_{epi\_31}(X - X_{epi}) + m_{epi\_32}(Y - Y_{epi}) + m_{epi\_33}(Z - Z_{epi})} \quad (9)$$

$$l_{(1*12)} = [X \ Y \ Z \ X_{epi} \ Y_{epi} \ Z_{epi} \ \omega_{epi} \ \phi_{epi} \ k_{epi} \ x_0 \ y_0 \ f]$$

$$\Sigma_{H(1*1)} = H_{Jacobi} \Sigma_{l(12*12)} H_{Jacobi}^T = [\sigma_{x_a}^2] \quad (10)$$

## 2.5 Point Cloud Refinement

This study implements the strategy mentioned in Section 2.4 by passing the disparity gained from low B/D pair into larger B/D ones. Through projecting the 3-D coordinates determined from matching in low B/D pair onto the images of larger B/D pairs, not only the uncertainty of searching region is reduced to support more efficient computation but also help find the conjugate image point pair with better intersection geometry in refining the point cloud as compared to the points produced in low B/D pair and larger B/D one without enforcing disparity delivery strategy. It may be followed to fuse the point clouds from low and large B/D pairs to comprehend the scene description taking the recorded attributes suggested in this study into consideration, thus the refinement in more general goal to highlight the salient features in the most simplified way with light data amount can be realized.

## 3. EXPERIMENTS AND RESULTS

### 3.1 Equipment and Image Acquisition

To verify the proposed method, an indoor scene 120 cm (height) x 70 cm (width) with depth of -0.659 m to -0.264 m for 3-D reconstruction in NTU lab, as shown in the images of Table 2, was deployed. Control points needed for orientation solution were measured by the Trimble M3 DR2 total station with distance precision about 3mm+2ppm and the angle precision 2". Images were acquired by Canon EOS70D camera and the exterior orientation with self-calibration was performed by Agisoft PhotoScan. The imaging configuration can be seen in Table 1 while Table 2 and Table 3 show the estimated orientation parameters and quality of observations, respectively, utilized for the test.

Table 1. Imaging configuration





	Image size (pixel)	480*720
	Pixel size (mm)	0.0317
	Principal distance (mm)	50
	Object distance (cm)	160-200
	GSD(mm)	1
	Overlap (%)	80
	Baseline (cm)	14.5

Table 2. Experimental datasets

Img 1	Img 2	Img 3
		
Position of exterior orientation (Unit: m)		
$X = -0.17064$	$X = -0.03905$	$X = 0.09875$
$Y = 0.47807$	$Y = 0.46538$	$Y = 0.43053$
$Z = -0.24116$	$Z = -0.23872$	$Z = -0.23838$

Pose of exterior orientation (Unit: °)		
$\omega = 82.52705$	$\omega = 82.66459$	$\omega = 82.52830$
$\phi = -14.33890$	$\phi = -12.67951$	$\phi = -10.69190$
$k = -0.67945$	$k = -0.67522$	$k = -0.55789$

The employed Agisoft PhotoScan does not give the quality information of orientation parameters. The authors considered the alignment result with the utilized control points and set the empirical errors of parameters, seen in Table 3, also regarded as observations in generalized least-squares adjustment sense for the follow-up processes.

Table 3. The observation errors

Observation	Error
Image point	$\pm 0.0317$ mm
Position parameter	$\pm 0.005$ m
Pose parameter	$\pm 0.0005$ °
Interior orientation parameter	$\pm 0.003$ mm

To implement the effective computation based on the algorithms proposed in this work, it is the authors' effort to develop the needed codes in MATLAB\_R2017b platform, including epipolar imagery generation, forward intersection, disparity delivery, and modification of SGM.

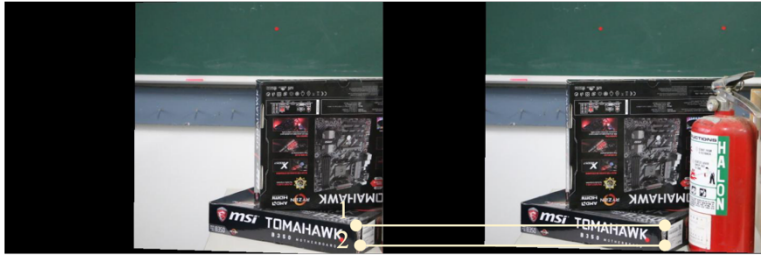
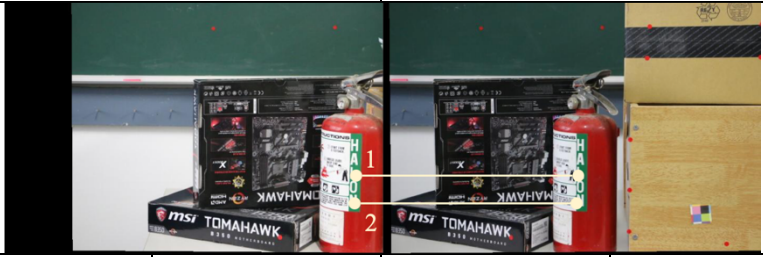
### 3.2 Generating Epipolar Images

The epipolar images were generated based on the procedures introduced in section 2.1. Two pairs, (Img\_1, Img\_2) and (Img\_1, Img\_3), with their pose parameters and errors were estimated and are given in Table 4. Note that the position parameters of the epipolar images remain the same as the original images because only rotation involves when transforming the original images to epipolar ones. To visually validate the row-to-row correspondence of epipolar images, the selected feature points shown in Table 5 confirm the satisfaction. To start with the SGM, initial disparity between Img\_1 and Img\_2 (Pair1) was set as 140 pixels and Img\_1 and Img\_3 (Pair2) 290 pixels based on the scene knowledge.

Table 4. Pose parameters and errors of epipolar images

	Pair1		Pair2	
	Value	Error	Value	Error
$\omega$ (°)	82.59585	$\pm 0.0004$	82.52770	$\pm 0.0004$
$\varphi$ (°)	-1.05738	$\pm 3.0641$	-0.58226	$\pm 1.4810$
$\kappa$ (°)	-5.50834	$\pm 3.0646$	-10.00825	$\pm 1.4811$

Table 5. Visual check of row to row correspondence

Feature point	point1		point2	
Epipolar image (Pair1)				
(row, column)	(428, 670)	(428, 530)	(468, 670)	(468, 530)
Disparity	140		140	
Epipolar image (Pair2)				
(row, column)	(330, 662)	(330, 372)	(376, 664)	(376, 375)
Disparity	290		289	



### 3.3 Disparity Delivery

To demonstrate how the proposed scheme works within limited pages, the reconstruction of adjacent plane features and geometric edges, as shown in Figure 4 (c), with about 85,000 points were highlighted for quality analysis.

**3.3.1 Assessment in low B/D pair:** According to the result of point clouds in low B/D pair, the maximum uncertainty in the depth direction is  $\pm 0.1039$  m. And the error propagation through projection finds about 14 pixels disparity uncertainty along the epipolar line in the larger B/D pair, a significant improvement in disparity approximation as compared to the value of 290 pixels without placing disparity delivery strategy. Thus much lighter computation load would be expected due to the effective support of disparity delivery.

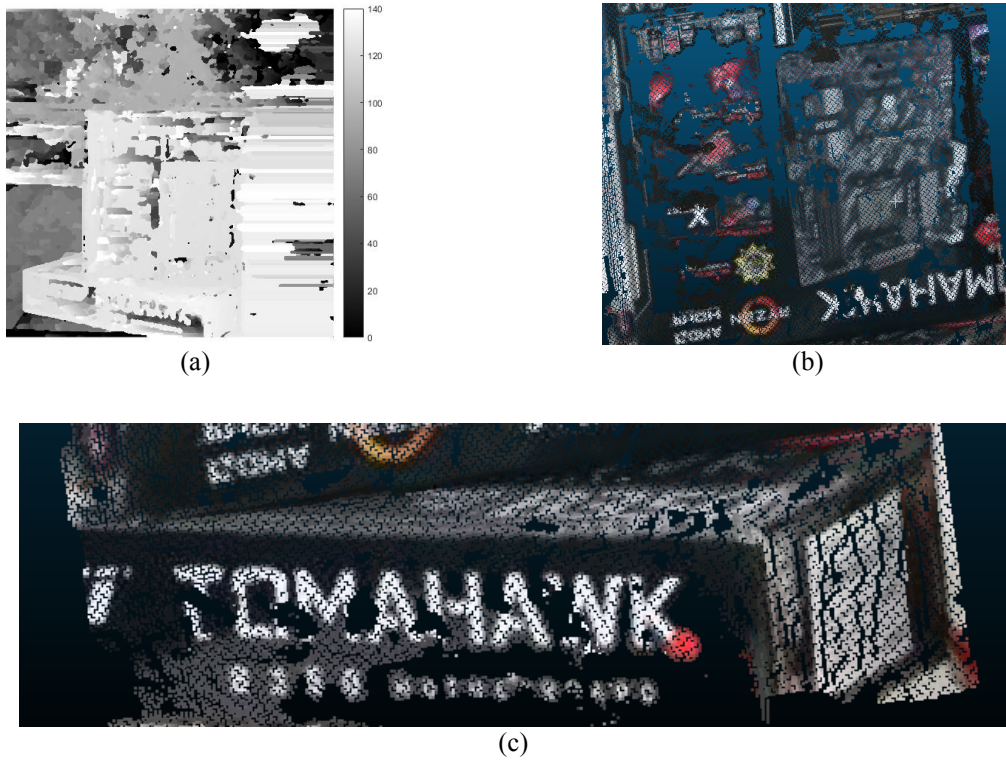


Figure 4. (a) The depth map of lower B/D pair; (b) The point clouds production in lower B/D pair; (c) The highlighted features

**3.3.2 Visual assessment:** Visual analysis of depth maps in Figure 5 elucidates that the proposed strategy performs better in rendering planes than the traditional method where disparity results only from scene knowledge. Besides, it also shows that the geometric edges are more preserved in the proposed method as compared to the traditional one (Figure 6). In our current implementation, disparities out of quality based on the error estimation bounded by the uncertainty determined through the proposed algorithms have been eliminated.

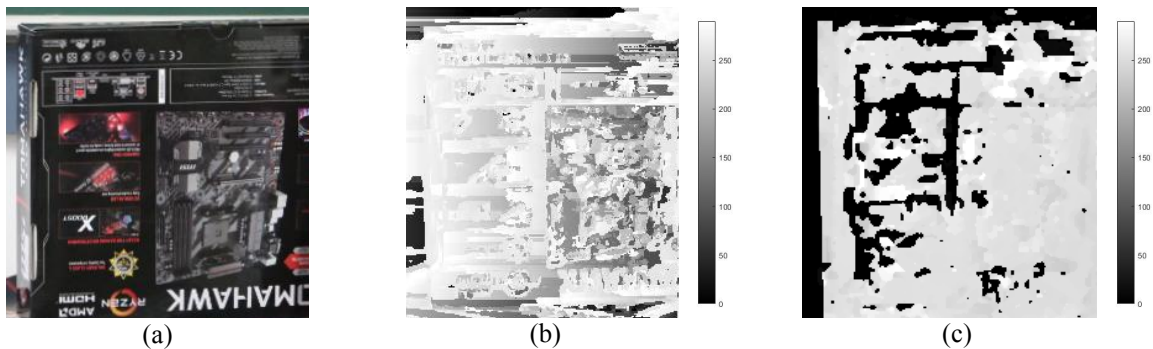


Figure 5. The highlight of a plane (a) the original image; (b) depth map by the traditional method; (c) depth map through the proposed strategy

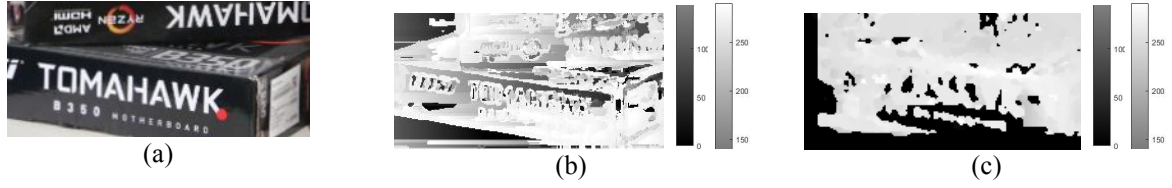


Figure 6. The highlight of geometric edge features (a) the original image; (b) depth map by the traditional method; (c) depth map through the proposed strategy

The number of points generated for large B/D pair in the traditional methods is about 33,827, one and half times less than the point number of area, thus most of matching results are considered as outliers. The fewer points, fragmented and hardly distinguishable, prevent the scene from even partially complete reconstruction. In contrast, with the proposed strategy, the total number of points is about 53,737, depicting the scene with more quality points and outlining the geometric features more explicitly, as seen in Figures 7 and 8. In other words, the proposed strategy can be used to provide the better geometric features with the improved quality and quantity of the point cloud.



Figure 7. Point clouds of a plane (a) by the traditional method; (b) through the proposed strategy

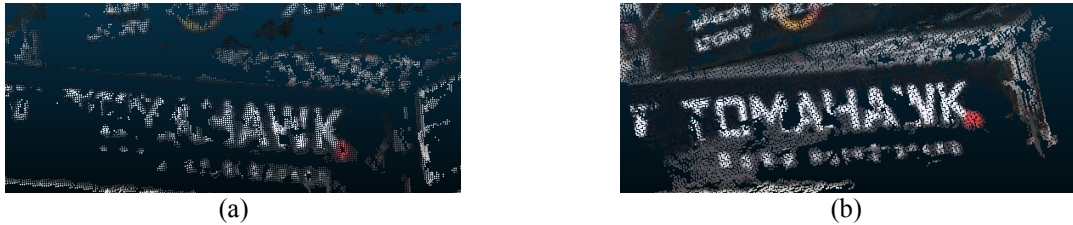


Figure 8. Point clouds of geometric edge features (a) by the traditional method; (b) through the proposed strategy

**3.3.3 Runtime analysis:** In addition to the qualitative performance of different procedures in depth map production, the runtime can also be an important issue to be analyzed. All codes developed in MATLAB were focusing on enabling the smooth computation of the proposed algorithms without putting too much effort into optimization goal. The runtime was measured on a 3.2 GHz Core CPU using the pair size of 480\*720 and the disparity range was given as 290 pixels in the traditional method, 14 pixels in the proposed strategy. As it can be seen in Table 6, the proposed strategy allows time savings up to seventy percent in the SAD algorithms, and ninety-six percent in SGM algorithms, which accounts for the vast majority of the whole computation.

Table 6. Comparison of runtime (Unit: Second)

	Traditional method	Proposed strategy
SAD	1.754025	0.549860
SGM	1395.432240	52.076873
Total	1421.759564	52.680165

#### 4. CONCLUSION AND SUGGESTION

Multi-view stereo matching provides tremendous observations through different pairs of images, bringing about complimentary scene information. This study proposes an effective disparity delivery strategy to accelerate the dense image matching and at the same time improve the point cloud in both quality and quantity. The primary tests demonstrate the promising results and encourage us to further work in gathering more pairs, as the practical situation,



with a general way of delivering disparity. Yet, at current stage, there is no valid evaluation method to illustrate the reliability of matching results, thus easily delivering invalid information to approximate conjugate point of larger B/D pair. The problem may find that the real conjugate point is not located in the given searching region. As a result, establishing complete matching algorithms to calculate correct and reliable disparity value and mechanism for detecting outliers are the key point in fully exploiting the proposed strategy.

Moreover, fusing the point clouds from low and large B/D pairs to comprehend the scene description taking the recorded attributes suggested in this study into consideration awaits implemented to refine the point cloud at the attribute levels that fit to the application needs.

## 5. REFERENCE

- Chiu, T.F., 2018. Subpixel Accuracy Image Edge with Quality Indicator Aided to Dense Stereo Matching, Nation Taiwan University, pp. 99. (in Chinese)
- Dall'Asta, E., and Roncella, R., 2014. A comparison of semiglobal and local dense matching algorithms for surface reconstruction, *ISPRS Journal of Photogrammetry and Remote Sensing*, Vol. XL, No. 5, pp. 187-194.
- Dominik, W., 2017. Exploiting the Redundancy of Multiple Overlapping Aerial Images for Dense Image Matching Based Digital Surface Model Generation, *Remote Sensing*, 9 (5), pp. 490.
- Haala, N., 2011. Multiray Photogrammetry and Dense Image Matching, *Proceedings of the Photogrammetric Week 2011*, University of Stuttgart, pp. 185-195.
- Hirschmüller, H., & Scharstein, D., 2009. Evaluation of stereo matching costs on images with radiometric differences. *IEEE transactions on pattern analysis and machine intelligence*, 31(9), pp. 1582-1599.
- Hirschmüller, H., 2008. Stereo Processing by Semiglobal Matching and Mutual Information, *IEEE Transactions on Pattern Analysis and Machine Intelligence*, 30 (2), pp. 328-341.
- Hirschmüller, H., 2005. Accurate and efficient stereo processing by semi-global matching and mutual information, *IEEE Computer Society Conference on Computer Vision and Pattern Recognition*, Vol. II, pp. 807-814.
- Liu, H.H., and Jaw, J.J., 2019. Refinement of dense image matching strategy and point cloud through multiple views, *International Symposium on Remote Sensing*, May, Taipei, Taiwan.
- Rothermel, M., Wenzel, K., Fritsch, D., and Haala, N., 2012. SURE: Photogrammetric Surface Reconstruction from Imagery. *Proceedings LC3D Workshop*, Berlin, December 2012.
- Topal, C., and Akinlar, C., 2012. Edge Drawing: A combined real-time edge and segment detector. *Journal of Visual Communication and Image Representation*, 23(6), pp. 862-872.
- Yan, L., Fei, L., Chen, C., Ye, Z., and Zhu, R., 2016. A Multi-View Dense Image Matching Method for High-Resolution Aerial Imagery Based on a Graph Network, *Remote Sensing*, 8 (10), 799.